Carbohydrate Polymers 192 (2018) 337–346

Contents lists available at ScienceDirect

Carbohydrate Polymers

journal homepage: www.elsevier.com/locate/carbpol

Preparation of nanocellulose from *Imperata brasiliensis* grass using Taguchi method

Kelly Cristina Coelho de Carvalho Benini[a,*], Herman Jacobus Cornelis Voorwald[a], Maria Odila Hilário Cioffi[a], Mirabel Cerqueira Rezende[b], Valdeir Arantes[c]

[a] Fatigue and Aeronautical Materials Research Group, Department of Materials and Technology, São Paulo State University (Unesp), School of Engineering, Guaratinguetá, 12516-410, São Paulo, Brazil
[b] Instituto de Ciência e Tecnologia, Unifesp - Univ. Federal de São Paulo, São José dos Campos, 12231-280, São Paulo, Brazil
[c] Biocatalysis and Bioproducts Laboratory, Department of Biotechnology, Lorena School of Engineering, University of São Paulo, Lorena, 12602-810, São Paulo, Brazil

ARTICLE INFO

Keywords:
Imperata brasiliensis fibers
Nanocellulose
Acid hydrolysis

ABSTRACT

Cellulose nanoparticles (CNs) were prepared by acid hydrolysis of the cellulose pulp extracted from the Brazilian satintail (*Imperata Brasiliensis*) plant using a conventional and a total chlorine free method. Initially, a statistical design of experiment was carried out using Taguchi orthogonal array to study the hydrolysis parameters, and the main properties (crystallinity, thermal stability, morphology, and sizes) of the nanocellulose. X-ray diffraction (XRD), fourier-transform infrared spectroscopy (FTIR), field-emission scanning electron microscopy (FE-SEM), dynamic light scattering (DLS), zeta potential and thermogravimetric analysis (TGA) were carried out to characterize the physical-chemical properties of the CNs obtained. Cellulose nanoparticles with diameter ranging from 10 to 60 nm and length between 150 and 250 nm were successfully obtained at sulfuric acid concentration of 64% (m/m), temperature 35 °C, reaction time 75 min, and a 1:20 (g/mL) pulp-to-solution ratio. Under this condition, the *Imperata Brasiliensis* CNs showed good stability in suspension, crystallinity index of 65%, and a cellulose degradation temperature of about 117 °C. Considering that these properties are similar to those of nanocelluloses from other lignocellulosics feedstocks, *Imperata* grass seems also to be a suitable source for nanocellulose production.

1. Introduction

Cellulose nanoparticles or nanocelluloses are cellulose elements with at least one dimension smaller than 100 nm (Habibi, Lucia, & Rojas, 2010; Siró & Plackett, 2010). In recent years, their use as cellulose nanofibrils (CNFs) or cellulose nanocrystals (CNCs) have attracted great attention for applications in sectors like pharmaceutical (Lee, Hamid, & Zain, 2014), biomedicine (Tehrani, Nordli, Pukstad, Gethin, & Chinga-Carrasco, 2016), electronic devices (Xiong et al., 2014) and as a reinforcement material in polymer nanocomposites (Ng et al., 2015) due to their unique properties such as high modulus (138–150 GPa), the ability to form a highly porous structure, large surface area, biodegradability and environmental benefits arising from their use (Cao et al., 2015; Kaushik, Singh, & Verma, 2010; Mariano, Cercená, & Soldi, 2016; Siró & Plackett, 2010; Saelee, Yingkamhaeng, Nimchua, & Sukyai, 2016).

There are various sources of cellulose in nature that can be used to isolate nanocelluloses. Among the sources, plant biomass is the most abundant and available and, therefore, offers the greatest potential for large scale production of both CNCs and CNFs. For example, nanocellulose has been successfully isolated from cellulose obtained from wood (Chen et al., 2011), mulberry pulp (Wang, Shankar, & Rhim, 2017), kenaf (Kargarzadeh et al., 2012), sugarcane bagasse (Mandal & Chakrabarty, 2011) and cotton (Martins, Teixeira, Corrêa, Ferreira, & Mattoso, 2011). However, it should be kept in mind that the properties of the nanocellulose (i.e. morphology, sizes, degree of polymerization) depend not only on the isolation method employed, but also on the source from which it was isolated (Habibi et al., 2010).

Imperata is a genus of tropical and subtropical grasses also known as satintail (Booth and Prior, 1984). *Imperata* grasslands and *Imperata*-infested areas are widespread in many countries (USDA, 2017). The Brazilian satintail (*Imperata brasiliensis Trin*) plant is actually considered an invasive plant found in degraded pastures and cultivated areas (Carvalho, Xavier, Freitas, & Silva, 2000). It is a monocotyledon that belongs to the group of angiosperm plants in the *Liliopsida* class, *Commelinidae* subclass and botanical family of *Poaceae* (USDA, 2017).

* Corresponding author.
E-mail address: benini@feg.unesp.br (K.C.C.d.C. Benini).

https://doi.org/10.1016/j.carbpol.2018.03.055
Received 5 January 2018; Received in revised form 23 February 2018; Accepted 17 March 2018
Available online 19 March 2018
0144-8617/

Brazilian satintail is native to southern North America, Central America, and South America, extending from the Cape Region of Baja California Sur, Mexico southward to Brazil and Argentina (Benini, Voorwald, Cioffi, Milanese, & Ornaghi, 2016). Despite its widespread abundance and occurrence, it does not present an industrial use (Carvalho et al., 2000), expect its use in dried form for making roofs of palapas on the Brazilian coastal region (Souza, Teixeira, & Torres, 1985). Therefore, *Imperata* still constitutes and abundant and underutilized natural resource.

Previously, promising results were obtained with micrometric scale *Imperata brasiliensis Trin* (IB) fibers when used as a reinforcement agent for thermoplastic composites (Machado, Sato, Mulinari, Cioffi, & Voorwald, 2009; Mulinari, Cioffi, & Voorwald, 2009). Recently, a detailed characterization study of IB found that IB fibers have similar chemical, physical and morphological properties of other lignocellulosic fibers that have successfully been used for isolation of nanocelluloses (Benini et al., 2016). These results suggest that *Imperata brasiliensis Trin* may be a suitable source of cellulose for nanocellulose production.

In order to assess the potential of the abundant and underutilized IB for isolation of nanocelluloses, this study first extracted cellulose from the IB plant by a total chlorine free method using alkaline and bleaching treatments and subjected the extracted cellulose to a sulfuric acid hydrolysis for isolation of the cellulose nanoparticles. The total chlorine free method was used in the process of isolation (bleaching step) of the cellulose, based on the fact that conventional processes, which make use of chorine based compounds, generate an effluent with organochlorine compounds of significant toxicity to plants, animals and humans (Rosa, Rehman, De Miranda, Nachtigall, & Bica, 2012; Seo & Kim, 2015) and it is not environmentally friendly (Lamaming, Hashim, Leh, & Sulaiman, 2017). Currently, due to these environmental problems, chlorine-free bleaching treatments with oxygen and oxygen based compounds such as hydrogen peroxide and ozone are being used as substitutes, since provide suitable results in the removal of amorphous constituents (Lamaming et al., 2017; Rosa et al., 2012; Seo & Kim, 2015). Although the acid hydrolysis with strong acid such as sulfuric acid is a well-known and commonly employed method to isolate cellulose nanoparticles (Habibi et al., 2010), it is also well known that the acid hydrolysis conditions greatly affect the final morphology, properties and yield of the nanoparticles (Kargarzadeh, Sheltami, Ahmad, Abdullah, & Dufrene, 2015; Teodoro et al., 2011). In this context, a statistical design of experiment was carried out using Taguchi orthogonal array to study the hydrolysis parameters, and the main properties (crystallinity, thermal stability, morphology, and sizes) of the nanocellulose obtained were determined.

2. Materials and method

2.1. Raw material

Brazilian satintail (*Imperata Brasiliensis*) plant was collected from farms located in Guaratinguetá, São Paulo state, Brazil, and used to obtain IB fibers. The major chemical composition was 37.7% cellulose, 35% hemicellulose, 14.3% total lignin and 13.8% extractives, as reported elsewhere (Benini et al., 2016).

2.2. Isolation of cellulose

Cellulose was extracted from IB fibers according to Benini et al. (2016). First, the fibers were treated with 5% (w/w) aqueous NaOH solution at 70 °C for 1 h under continuous stirring. In order to remove the residual lignin, an environmentally friendly bleaching method (chlorine free) was employed. Thus, the alkali treated fibers were bleached three times with a 1:1 solution of H_2O_2 (24% v/v) and NaOH (4% w/w) at 50 °C under constant stirring for 2 h. After each treatment, the suspension was filtered and washed with distillated water to reach neutral pH. Fibers were then dried at 60 °C for 48 h. The fiber:solution ratio used in all treatments was 1:20 (g/mL). The chemical composition of the bleached fibers, determined according to the procedure used by Benini et al. (2016), was 83.4% cellulose, 9% hemicellulose and 7.6% lignin.

Table 1
Selected processing parameters (factors), their respective levels and the Taguchi L9 orthogonal array design.

Factors		Levels		
		1	2	3
(A) H_2SO_4 concentration (wt%)		50	60	64
(B) Reaction time (min)		30	60	75
(C) Pulp:solution ratio (g/mL)		1:15	1:20	1:50
(D) Temperature (°C)		35	55	60
Experiment	Abbreviation	Variables and Levels		
		A	B	C	D
1	CN 1	1	1	1	1
2	CN 2	1	2	2	2
3	CN 3	1	3	3	3
4	CN 4	2	1	2	3
5	CN 5	2	2	3	1
6	CN 6	2	3	1	2
7	CN 7	3	1	3	2
8	CN 8	3	2	1	3
9	CN 9	3	3	2	1

2.3. Preparation of cellulose nanoparticles

Isolation of CNs was carried out by acid hydrolysis of the bleached IB fibers (5 g) according to a statistical design of experiment using the Taguchi Orthogonal array of L9 (3^4) method to minimize the number of experiments but still obtain information of the following processing parameters: (A) sulfuric acid concentration; (B) reaction time, (C) pulp-to-solution ratio; and (D) temperature. Each of these variables was tested at three levels (1, 2 and 3) (Table 1).

The resulting suspension after each acid hydrolysis was centrifuged at 5.000 rpm for 30 min and dialyzed with a tubing membrane (MWCO 12000–14000, 20 mm diameter, SERVAPOR®) using distilled water until a neutral pH was reached. The colloidal suspensions were sonicated in an ultrasonicator (VCX 750, Sonics and Materials model) at 20 kHz frequency and 750 W, for 5 min in an ice-bath to avoid heat-up. Suspensions were then stored in a refrigerator with a few drops of chloroform ($CHCl_3$) to prevent the bacterial growth. Yield of CNs obtained for each sulfuric acid hydrolysis condition was calculated by the determination of dry content as described by Arrieta et al. (2014).

2.4. Characterization

2.4.1. X-ray diffraction (XRD)

Diffractograms of the cellulose nanoparticles (CN) were obtained on a Shimadzu diffractometer (XDR-6000 model), operating at 40 kV, 30 mA and CuKa radiation (l = 0.1542 nm). First, a sample of the aqueous CN suspensions was oven dried at 30 °C for 24 h. Then, the dried samples were scanned in 2θ ranges varying from 10 to 30° (2θ/5 s). Results of interplanar distance (d-spacing) and crystallite size (L) for different crystalline planes were evaluated, as well as the total crystallinity index (CI). Deconvolution of the peaks was initially performed to check the contribution of each crystalline plane. The deconvolution was developed according to the standard crystallographic cellulose Iβ, which was inserted into Mercury 3.0 software program from the Cambridge Crystallographic Data Centre (public domain) provided in the digital supplementary material in French (2013).

The d-spacing of each plane was calculated using Braggs law

($n\lambda = 2d \sin\theta$) and the crystallite size (L) was obtained by the Scherrer equation (Eq. (1)) (Poletto, Ornaghi, & Zattera, 2014):

$$L = (0.94\lambda)/(H \cos\theta) \quad (1)$$

where, L is the crystallite size perpendicular to the plane, λ is the X-ray wavelength (0.1542 nm), H is the full-width at half-maximum in radians, and θ is the Bragg angle in radians.

The CI was calculated by the Segal's empirical method (Segal, Creely, Martin, & Conrad, 1959), according to Eq. (2):

$$CI = \frac{I_{(200)} - I_{(am)}}{I_{(200)}} \times 100 \quad (2)$$

where $I_{(200)}$ is the maximum intensity of the diffraction from the (200) lattice peak at $2\theta \approx 22^{\circ}$ and $I_{(am)}$ is the intensity of the amorphous material diffraction, which is taken at $2\theta \approx 18–19^{\circ}$, where the intensity is at the minimum.

2.4.2. Fourier transform infrared (FTIR) spectroscopy

To evaluate the functional groups in the IBB fibers and NCs surface, the attenuated total reflection (ATR) technique was used. Fibers spectra were determined in a Spectrun GX Perkin Elmer spectrophotometer by taking 8 scans in the range of 4000–800 cm^{-1}, with a resolution of 4 cm^{-1}.

2.4.3. Thermogravimetric analysis (TGA)

The thermal degradation of the CN samples (approximately 10 mg on a dry weight) was analyzed with a TG/DTG SII Nanotechnology INC (6200 model) at a heating rate of 10 °C min^{-1} under nitrogen flow of 60 mL/min, ranging from 25 °C to 550 °C. The initial degradation temperature was determined from the first inflection of the baseline in the differential thermogravimetric (DTG) curve, according to ASTM E2550.

2.4.4. Electron microscopy

The morphology of the cellulose nanoparticles was analyzed by Field-emission scanning electron microscopy (FE-SEM), performed on a Scanning Electron Microscope (JEOL, 7500F), equipped with electron gun type Field Emission (theoretical resolution of 1 nm), under accelerated electrons with 2 kV. Initially, the aqueous CN suspensions were diluted (10 times) and one drop of each suspension was dried at room temperature on a glass substrate and then covered by carbon evaporation. The diameters of the NCs were measured with the aid of public domain software *Image J*.

2.4.5. Particle size measurements and Zeta potential

The average hydrodynamic particle size and surface charge (Zeta potential) of the CNs in aqueous suspension were determined by Dynamic Light Scattering (DLS) using the particle size analyzer DelsaNano (Beckman Coulter Zeta, Delsa™ Nano C). Particles were analyzed in a range of 0.6 nm to 7 μm in the following conditions: water refractive index 1.3328; viscosity 0.8878 mPas; angle 15° and temperature 25 °C. All analyses of the sonicated CN suspensions were carried out in triplicated.

3. Results and discussion

In order to obtain cellulose nanoparticles from the cellulose extracted from *Imperata brasiliensis* (IB) fibers, nine experimental conditions for the acid hydrolysis were tested according to the experimental design shown in Table 1. Among the final suspensions obtained, it was visually observed that only suspensions 1 (CN 1) and 2 (CN 2) had high amount of non-hydrolyzed fibers. In order to separate micrometric from submicrometric fibers, these two suspensions were further filtered with a qualitative filter paper 80 g/m^2 before ultrasonication. The two suspension filtrates were totally transparent, indicating that cellulose nanoparticles were likely absent in the aqueous suspensions. The absence

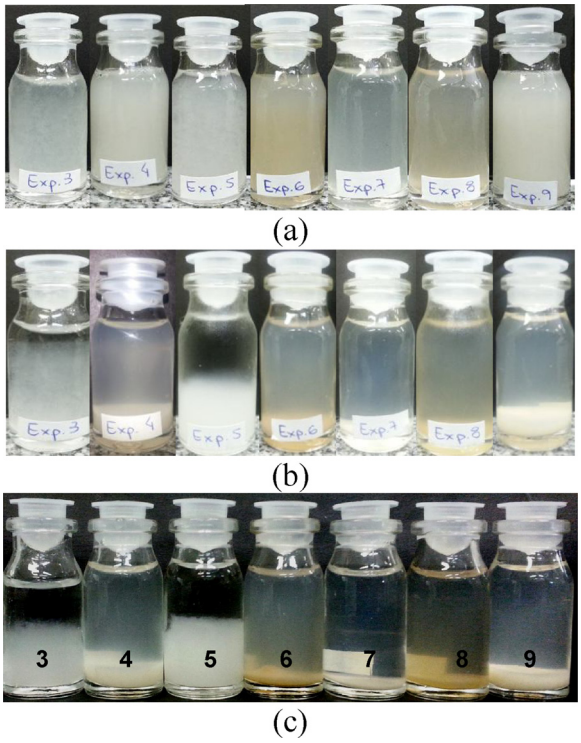

Fig. 1. Images of the CN suspensions obtained under different acid hydrolysis conditions. Experimental conditions after ultrasonication: (a) t = 0, (b) t = 7 days and (c) t = 60 days.

of cellulose nanoparticles is likely due to the mild hydrolysis conditions employed in CN 1 and CN 2 experiments. Therefore, the suspensions obtained with these two conditions were not considered for subsequent characterization analyses.

The stability of the aqueous CN suspensions was initially assessed by visual inspection of the suspensions over a period of 60 days after ultrasonication (Fig. 1). The visual analysis of the suspensions provides important information about the acid hydrolysis efficiency, since a turbid supernatant with low amount of decanted particles is a strong indicator of the presence of cellulose nanoparticles (Frone et al., 2011). In addition, decanted particles can be associated to the presence of large fibers and/or low amount of sulfate groups on the fiber surface (Santos et al., 2013). CN suspensions 4, 6, 7, 8 and 9 exhibited high turbidity (Fig. 1a) and low amount of non-hydrolyzed fibers (settled fibers) after seven (t = 7) (Fig. 1b) and sixty (t = 60) days (Fig. 1c). Turbidity was not observed in CN suspensions 3 and 5 (Fig. 1a), but a complete phase separation could be observed after seven (Fig. 1b) and sixty days (Fig. 1c).

The yellowish color that can be observed in CN suspensions 6 and 8 suggests that cellulose degradation may have occurred during hydrolysis and/or the presence of residual organic substrates, including lignin and hexenuronic groups (Qua, Hornsby, Sharma, & Lyons, 2011). According to Heggset et al. (2017), cellulose degradation with concomitant color-change occurs due to the formation of carbonyl groups in the cellulose chains, and also due to the formation of colored low-molecular furan-type compounds during the thermal degradation of carbohydrates.

The yield of CNs according to acid hydrolysis conditions was 45%, 43%, 39%, 38%, 37%, 36% and 43% for CN 3 to CN 9, respectively. These values are higher than that reported in literature for nanocelulose obtained by other methods. For example, the yield varied from 7.8% to 27.6%, according to time and power of sonication for nanocellulose isolated from microcrystalline cellulose by sonication (Frone et al., 2011), Arrieta et al. (2014) obtained yield of 20.6% for cellulose nanocrystals obtained from microcrystalline cellulose by sulphuric acid

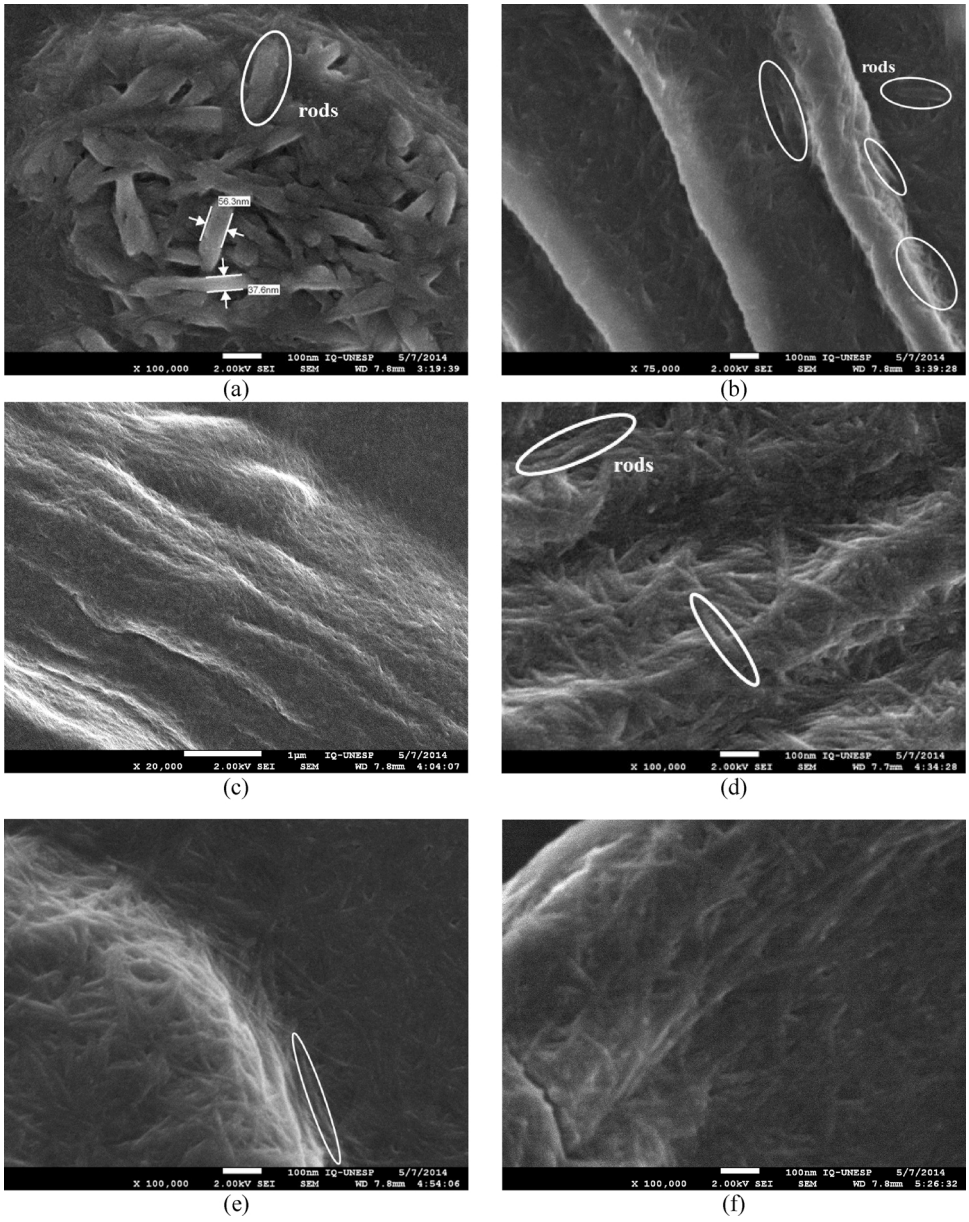

Fig. 2. FE-SEM micrographs of the CNs obtained under different acid hydrolysis conditions. Experimental conditions 3 (a), 4 (b), 6 (c), 7 (d), 8 (e), and 9 (f).

hydrolysis carried out with 64% (w/w) at 45 °C for 30 min, and Goh, Ching, Chuah, Abdullah, and Liou (2015) obtained yield of 25% for acid-hydrolysis of microfibrillated celluloses and 40% for microfibrillated celluloses extracted via ammonium persulfate (APS) oxidation.

3.1. FE-SEM analysis

It appears that the hydrolysis condition CN 5 was not efficient to disrupt the cellulose fiber structure and isolate cellulose nanoparticles as the fibers released under CN 5 condition were still in the micrometric scale (data not shown).

For the acid hydrolysis conditions CN 3, 4, 6, 7, 8 and 9 that lead to the release of cellulose nanoparticles, the FE-SEM micrographs are shown in Fig. 2. All these hydrolysis conditions resulted in a network like structure. This network-forming ability is an important characteristic of nanocelluloses as it is associated to strong reinforcement when used in polymeric composites (Tian et al., 2016). In addition, these hydrolysis conditions also led to the isolation of nanoparticles with diameter and length within 10–60 nm and 150–250 nm, respectively. Yu et al. (2012) also reported particles with dimensions in the order of 20 nm diameter and 230 nm length and similar morphology (in the form of rods) after acid hydrolysis of microcrystalline cellulose.

The suspension obtained under CN 3 condition contained nanoparticles (Fig. 2a), but showed no turbidity (Fig. 1a), indicating the low stability of the CN suspension. Stable suspensions means that cellulose nanoparticles are not decanted. Consequently the dispersion of theses nanoparticles on the suspension are responsible for the turbidity. According to Rosa et al. (2010), the higher the nano/microfibril ratio, the better the dispersion and stability of aqueous nanocellulose suspension. Therefore, it is possible that the nanofibrils/microfibrils ratio in suspension CN 3, and possibly in suspension CN 5 as well, is lower than in the other suspensions.

The presence of micrometric fibers with lengths within the range of 13 and 60 μm and diameter between 3 and 9 μm were observed for the suspension obtained under CN 6 hydrolysis condition.

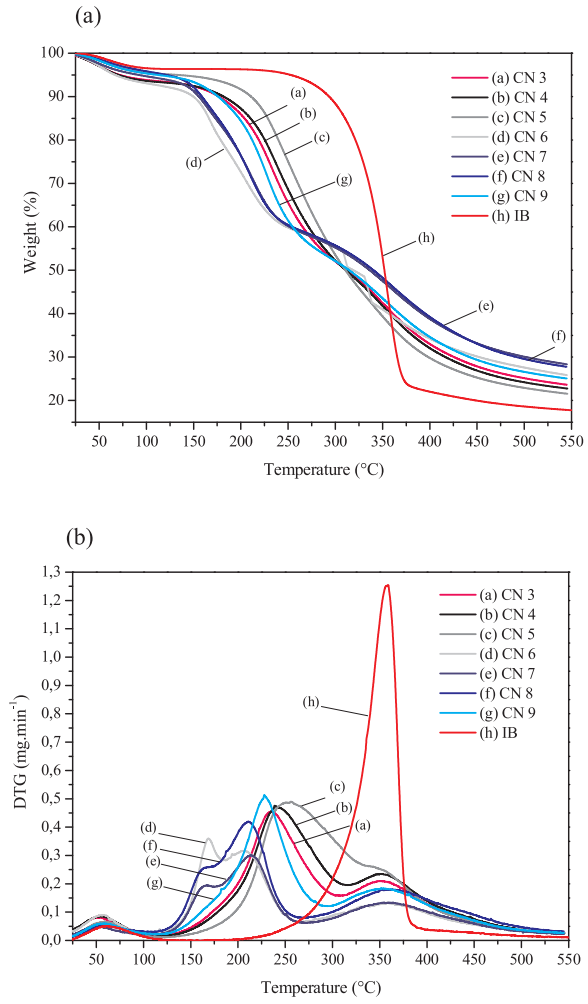

Fig. 3. Thermogravimetric curves of the IB and CNs obtained under different processing conditions: (a) TGA and (b) DTG.

3.2. Thermal analysis

Thermogravimetric curves and the thermal parameters of IB fibers and the cellulose nanoparticles obtained under the different hydrolysis conditions are shown in Fig. 3 and in Table 2, respectively. As expected, the presence of sulfate groups, that is very well known to be bound on the surface of nanocellulose isolated by sulfuric acid hydrolysis, decreased the thermal stability of the isolated nanoparticles (108 °C to 125 °C) in relation to IB fibers (200 °C).

The first degradation stage, due to evaporation of moisture, occurred between 25 °C and 125 °C for all the samples, and corresponded to a weight loss in the range of 3.4% (IB) to 7.8% (CN 6) (Mtibe et al., 2015). After water evaporation, IB fibers displayed only one cellulose degradation peak ranging from 200 °C to 400 °C, corresponding to a weight loss of 74.3%. On the other hand, the cellulose nanoparticles isolated under CN 6–8 conditions showed three distinct stages of cellulose degradation, whereas nanoparticles isolated under conditions CN 3–5 and CN 9 showed two stages with temperature ranging between 108 °C and 550 °C.

The first peak of cellulose degradation that occurs at lower temperatures (around 167 °C) only for CN 6–8 refers to the most accessible regions of the amorphous cellulose, where the presence of sulfate groups is higher. The other peak (between 208 °C to 254 °C), for all cellulose nanoparticles, is related to the pyrolysis of crystalline regions of cellulose, which is less easily accessed by sulfuric acid (Teodoro et al., 2011; Wang et al., 2017). The effect of sulfate groups in the thermal stability of nanocellulose was also observed by Boujemaoui, Mongkhontreerat, Malmström and Carlmark (2015), Mtibe et al. (2015) and Mariano, Cercená and Soldi (2016), and it is related to the presence of sulfate groups that catalyzes the thermal degradation of cellulose (Martins et al., 2011).

Table 2
Weight loss and degradation temperatures of the IBB and CNs obtained under different hydrolysis conditions.

Samples	ΔT (°C)	T_{peak} (°C)	T_i (°C)	Weight loss (%)	Residue at 550 °C (%)
IB	25–125	65	200	3.4	17.2
	200–400	360		74.3	
	400–550	425		4.8	
CN 3	25–120	52	120	6.6	23.6
	120–310	235		43.1	
	310–550	352		26.7	
CN 4	25–125	56	125	6.9	22.7
	120–315	242		43.9	
	315–550	351		26.5	
CN 5	25–125	59	125	4.9	21.6
	125–335	254		51.9	
	335–550	350		21.7	
CN 6	25–108	57	108	7.8	25.8
	108–188	169		15.4	
	188–278	208		19.3	
	278–550	358		31.7	
CN 7	25–117	50	117	5.6	28.3
	117–175	167		9.9	
	175–271	214		26.4	
	271–550	400		29.7	
CN 8	25–114	59	114	4.5	27.8
	114–175	167		10.2	
	175–270	211		26.7	
	270–550	364		30.8	
CN 9	25–117	57	117	5.2	25.1
	117–295	229		42.1	
	295k550	355		27.7	

The last degradation stage, which occurred at a temperature above 270 °C for all cellulose nanoparticles samples, and above 400 °C for IB fibers, is related to the degradation of carbonaceous residues, decomposition of monomeric d-glucopyranose units into free radicals responsible for the presence of residual ashes (Barud et al., 2011; Kalita et al., 2015). The weight loss in the third stage of cellulose degradation varied from 4.8% (IB) to 31.7% (CN 6). In addition, degradation above 400 °C can be attributed to the decomposition of amorphous components of cellulose, presence of residual lignin and/or cellulose–lignin complex (Kalita et al., 2015; Mtibe et al., 2015).

The final residues at 550 °C were higher for the nanoparticles (≈25%) than for IB (17.2%). This is likely due to the sulfate ester groups that act as flame retardant (Wang et al., 2017).

3.3. FTIR analysis

The FTIR spectra of IB and the cellulose nanoparticles obtained under different hydrolysis conditions are shown in Fig. 4a. Two main absorption regions in the ranges of 2800–3600 cm^{-1} and 750–1750 cm^{-1} were observed in the spectra. In general, FTIR spectrum analysis reveals that major changes among the cellulose nanoparticles obtained under different hydrolysis conditions were not observed. In addition, they showed similar pattern, which is similar to the spectrum pattern reported for cellulose nanowiskers obtained from kenaf (Kargarzadeh et al., 2012) and flax (Qua et al., 2011).

A broad band in the region 3334 cm^{-1}, observed for all samples, indicates the O—H free stretching vibration of the CH_2—OH structure on cellulose (Xiang, Gao, Chen, Lan, & Troy, 2016) and OH groups which correspond to intra and intermolecular hydrogen bonds present in cellulose and absorbed water (Sheltami, Abdullah, Ahmad, Dufresne, & Kargarzadeh, 2012; Dai & Fan, 2011). This band is more evident in the

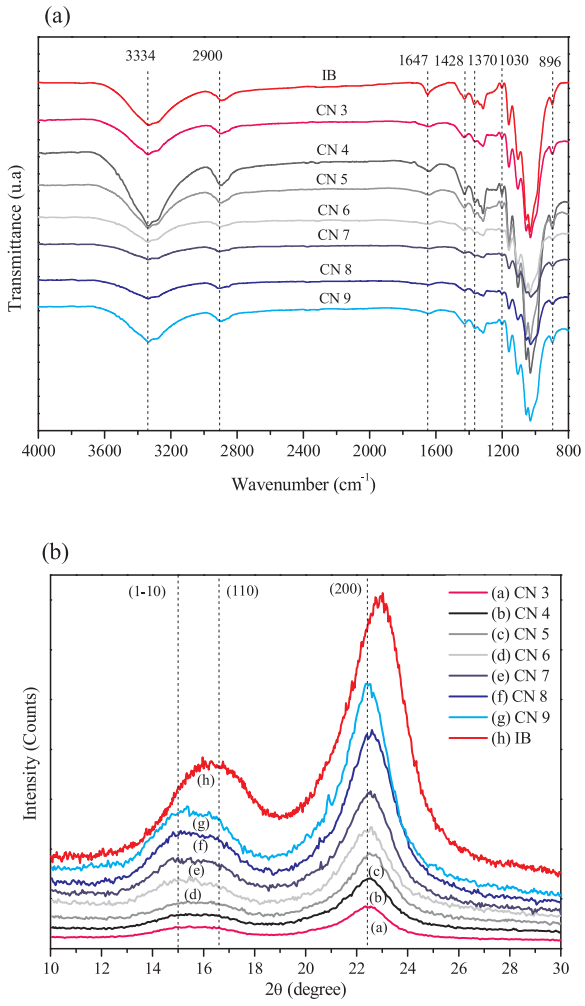

Fig. 4. FTIR spectra (a) and X-ray diffraction patterns (b) of IB and CNs obtained under different hydrolysis conations.

spectrum of the nanoparticles obtained under CN 4 (the highest reaction time) and CN 9 (the highest acid concentration) conditions, indicating a high exposure of cellulose. The peaks around 2900 cm^{-1} are due to C—H stretching vibration in cellulose and hemicellulose and peaks located at 1647 cm^{-1} are attributed to bending vibrations of the OH groups of cellulose (Kargarzadeh et al., 2012; Mandal & Chakrabarty, 2011).

The bands observed at 1428 cm^{-1} are related to the C=C stretching and/or CH_2 symmetric bending in aromatic groups of cellulose due to crystallinity band (Saelee et al., 2016; Wang et al., 2017; Shankar & Rhim, 2016; Kargarzadeh et al., 2015). The spectra of the cellulose nanoparticles obtained under CN 6–8 conditions show a significant reduction in the intensity of this crystallinity band compared to the nanocelluloses obtained under other hydrolysis conditions. This result indicates that these hydrolysis conditions might have decreased the crystallinity level of the nanocelluloses, as observed for the DRX results, with exception of CN 8.

The absorbance band at 1030 cm^{-1} is associated to C—O stretching and C—H rocking vibration of pyranose ring skeletal (Kargarzadeh et al., 2012). The 896 cm^{-1} band in the spectra corresponds to ß-glycosidic links between the glucose units of cellulose (Mandal & Chakrabarty, 2011). The presence of this band in the CN spectra is interesting, since it is an indicative that cellulosic material may have not been lost during the acid hydrolysis. Peaks in the range of 1500–1660 cm^{-1} are associated to proteins (Xiang et al., 2016), and their absence indicates that the cellulose extracted from IB fibers is free of proteins.

3.4. XRD analysis

X-ray diffractograms of IB and the cellulose nanoparticles obtained under different hydrolysis conditions are shown in Fig. 4b. All diffractograms contained two intense peaks, one at 16° and the other at 22°. The peak at $2\theta \approx 16°$ corresponds to crystallographic planes, overlapping ($1\bar{1}0$) and (110) peaks, characteristic of crystallographic semicrystalline materials, such as lignocellulosic fibers. The peak at $2\theta \approx 22°$ corresponds to the (200) plane, characteristic of crystalline cellulose polymorphism Iβ (Martins et al., 2011; French, 2013). It can be seen that the position of the peaks is not in full agreement with theoretical values for the crystal planes ($1\bar{1}0$), (110) and (200) at $2\theta \approx 14.88°$, 16.68° and 22.9°, respectively. According to French (2013) the observed shift of the peaks can be attributed to crystallite size variations which result in different long-range compressive forces on the crystals and unit cells.

The two peaks at 2θ near 16° are best viewed in XRD patterns of lignocellulosic fibers with high cellulose content, such as curaua and cotton (Ornaghi, Poletto, Zattera, & Amico, 2014). For other lignocellulosic fibers, as in the case of the IB fibers, the presence of only one peak is detected. Peaks overlapping occurred because cellulose is hidden by amorphous and non-cellulosic components such as lignin, hemicellulose and amorphous cellulose (Spinacé, Lambert, Fermoselli, & Paoli, 2009).

Crystallinity index values (CI), crystallite size perpendicular to each of the three main planes (L) and interplanar distance (d-spacing) for each crystallographic plane are shown in Table 3. The crystallographic planes ($1\bar{1}0$), (110) and (200) are identified with the indexes 1, 2 and 3, respectively. The d-spacing values are important because they can provide information on changes in the type of cellulose (Iα and Iβ), since crystal structures are different (triclinic and monoclinic). The crystallite size (L) is an indicative of the material stiffness and varies with the cellulose content (Wada & Okano, 2001).

Compared to the IB fibers, the acid hydrolysis lead to an increase in the d-spacing values for the ($1\bar{1}0$) and (110) planes and also for crystallite size L3, and a small increase in CI for the cellulose nanoparticles obtained under acid hydrolysis conditions CN 3–5 and CN 8–9 (Table 3). The interplanar distance values for the three crystallographic planes did not change significantly after acid hydrolysis of IB fibers. The values obtained for the nanoparticles were similar to those obtained for microcrystalline cellulose (*Cladophora sp.)* treated with sulfuric acid 60% (w/w) (Wada & Okano, 2001) and for a structural model of cellulose I (Elazzouzi-Hafraoui et al., 2008).

The crystallite sizes were more sensitive to the hydrolysis conditions, particularly the (110) plane, with L2 ranging from 5.28 nm to 8.39 nm. The (110) plane contains more O—H groups than the ($1\bar{1}0$) plane (Olaru, Malutan, Ursescu, Geba, & Stratulat, 2016) and are more susceptible to changes during the acid hydrolysis. In general, the lower value of L2 and the higher value of crystallinity index of the

Table 3
Crystallinity parameters of IB and CNs obtained under different hydrolysis conditions.

Samples	d-spacing (nm)			Crystallite (nm)			CI (%)
	d1	d2	d3	L1	L2	L3	
IB	0.57	0.52	0.39	5.34	6.22	3.59	62
CN 3	0.59	0.54	0.40	5.37	**5.95**	4.68	**67**
CN 4	0.59	0.54	0.39	5.62	6.41	4.23	**65**
CN 5	0.59	0.54	0.39	5.08	6.61	4.34	**65**
CN 6	0.60	0.55	0.39	5.48	**5.28**	4.26	61
CN 7	0.60	0.54	0.39	5.51	**8.39**	4.23	60
CN 8	0.59	0.54	0.39	5.27	6.17	4.28	**65**
CN 9	0.59	0.54	0.40	5.27	7.17	4.84	**65**

nanocelluloses indicate that the hydrolysis of IB fibers was effective, expect for the nanoparticles CN 6–7 that had the lowest and the highest L2 value, respectively, but the lowest CI values. Considering the suspension color (yellowish), reaction time (75 min) and the TGA results (two cellulose degradation peaks and T_i = 108 °C) for the nanoparticles obtained under CN 6 condition, the reduction in the CI can be related to the degradation of crystalline cellulose. On the other hand, the reduction in the CI for the CN 7 condition can be related to the lack of sulfonation, which corroborates with the higher degradation temperature and higher crystallite size observed as compared to the CN 6 condition. Although condition CN 7 was carried out with a higher acid concentration, the reaction time (30 min) was considerably shorter than for CN 6 condition (Table 1), which justifies the fact that sulfonation process was not effective for the CN 7 condition. These findings suggest that the variables reaction time and temperature had higher influence on the L2 values than the acid concentration.

Considering the CI of bleached IB fibers and its CNs, it is important to highlight that the values are in agreement with values reported in the literature for cellulose obtained from Ushar (*Calotropis procera*) seed fibers (57%) (Oun & Rhim, 2016) and alkali treated and bleached citrus waste fibers (50%) (Mariño, Lopes da Silva, Durán, & Tasic, 2015). Niu et al. (2017) reported that the CI of the cellulose extracted from microcrystalline cellulose increased from 49.7% to 72.3% as the hydrolysis (with sulfuric and hydrochloric acid) time increased (0–10 h). However, this CI value is lower than that obtained for bleached fibers (77.3%) and bleached nanoparticles (81.4%) from kenaf, containing about 0.5% lignin (Jonoobi, Harun, Shakeri, & Misra, 2009). Thus, the low values of CI obtained for bleached IB fibers and IB CNs can be explained based on the fact that although the IB fibers were subjected to pre-chemical treatments before acid hydrolysis, they still contained a considerable amount of residual lignin (7.6%), an amorphous material.

Reaction time has also been shown to influence the CI. Rosa et al. (2010) reported that samples hydrolyzed for 120 min had the highest CI (65.9%) as compared to samples hydrolyzed 150 (CI 62.2%) and 180 (62.5%) min. These CI reductions occur due to the prolonged hydrolysis that removes not only the amorphous regions, but also destroys partially the crystalline domains (Rosa et al., 2010).

For the nanocelluloses obtained under other hydrolysis conditions CN 3 and CN 9, the CI values were 67% and 65%, respectively. That is, higher than the unhydrolyzed IB fibers (CI 62%). It is possible that although CN 3 samples has been obtained at lower acid concentration (50% w/w) in comparison to CN 9 (64%), the reaction time was the same (75 min), however the temperature was higher than for CN 3, which may have led to a high CI value. These two hydrolysis conditions also led do nanocelluloses with the best results in the TGA analyses, considering a more homogeneous (only two cellulose degradation peaks) and effective sulfonation (lower initial degradation temperature) (Fig. 4a).

3.5. Selection of acid hydrolysis conditions for nanocellulose production

A summary of the physical-chemical properties of the suspensions obtained after the acid hydrolysis of the IB fibers under the nine different conditions (CN 1–9) is shown in Table 4, and was used for comparative analysis in order to determine the acid hydrolysis condition more suitable for isolation of cellulose nanoparticles from IB fibers.

The lowest acid concentration tested (50% w/w) was not efficient for isolation of cellulose nanoparticles. At 50% (w/w) acid, particles were only observed for condition CN 3, corresponding to the longest reaction time (75 min) and the highest reaction temperature (60 °C). Nevertheless, the CN 3 suspension did not show good stability (Fig. 1a). With an increase in acid concentration to 60% (w/w), conditions CN 4–6, it was possible to obtain nanoparticles for conditions CN 4 and CN 6. However, CN 6 suspension had a yellowish color (Fig. 1) and low values for Ti and CI (Tables 2 and 3, respectively). Therefore, it seems that at an acid concentration of 60%, the condition CN 4 is more suitable for isolation of cellulose nanoparticles from IB fibers. At the highest acid concentration tested (64% w/w), all three conditions (CN 7–9) were efficient for isolation of nanocellulose. However, CN 9 condition yielded a turbid and stable suspension, and nanoparticles with the highest CI (64.5%), high T_i value (117 °C) and only one cellulose degradation peak (Fig. 4a), indicating a more homogeneous sulfonation (Teodoro et al., 2011).

As a resulted of the distinguished properties of the nanocelluloses obtained from IB fibers for the acid hydrolysis conditions CN 3, 4 and 9, they were selected for further characterization.

3.6. Particle size and distribution

Dynamic Light Scattering (DLS) is a widely used method to obtain the statistical size distribution of cellulose nanoparticles in suspension. However, it is important to highlight that DLS measurements consider that all the particles are spherical and the size values depend on the orientation of the fibers in suspension (Frone et al., 2011). As the nanocelluloses obtained in this work have an elongated morphology according to the FE-SEM analysis (Fig. 2), the sizes reported are approximations of real size values, but are adequate for comparison studies among different samples (Frone et al., 2011).

Measures obtained by DLS are in most cases higher than size values obtained by microscopy (Shankar & Rhim, 2016). This difference occurs because for microscopy analysis, physical measurements of dry particles are performed, while for DLS analysis, the particle hydrodynamic diameter in suspension is measured, and, as these particles have high hydrophilicity and quickly aggregate in suspension, values significantly higher are commonly observed (Adsul, Soni, Bhargava, & Bansal 2012; Zhou, Fu, Zheng, & Zhan, 2012).

The minimum and maximum values for each group of particles, considering intensity (Fig. 5a) and number (Fig. 5b), as well as values for polydispersity index (PDI) and Zeta potential are shown in Table 5. Particle size distribution with regard to signal intensity provides information about the entire sample and is obtained directly from measurements performed by the equipment. On the other hand, particle size distribution regarding the number of particles is derived from the intensity data and is used to estimate the relative amount of material in

Table 4
Comparison of CNs properties obtained under different acid hydrolysis conditions.

Condition	H_2SO_4 (%)	Time (min)	Ratio (pulp:solution)	Temp. (°C)	Ti (°C)	CI (%)	L2 (nm)	Appearance	Suspension Stability
CN 1	50	30	1:15	35	–	–	–	transparent	–
CN 2	50	60	1:20	55	–	–	–	transparent	–
CN 3	**50**	**75**	**1:50**	**60**	**120**	**67**	**5.95**	**turbid**	**unstable**
CN 4	**60**	**30**	**1:20**	**60**	**125**	**65**	**6.41**	**turbid**	**stable**
CN 5	60	60	1:50	35	125	65	6.61	turbid	unstable
CN 6	60	75	1:15	55	108	61	**5.28**	turbid/yellowish	stable
CN 7	64	30	1:50	55	117	60	8.39	turbid	stable
CN 8	64	60	1:15	60	114	65	6.17	turbid/yellowish	stable
CN 9	**64**	**75**	**1:20**	**35**	**117**	**65**	**7.17**	**turbid**	**stable**

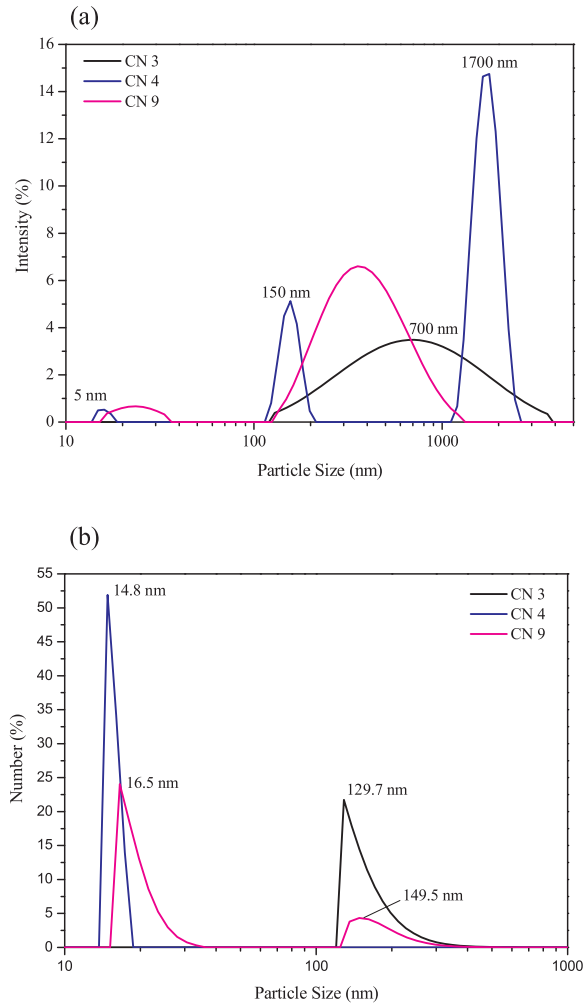

Fig. 5. CNs size distribution by DLS (a) signal intensity and (b) number of particles.

each peak separately, and the diameter values are less reliable.

With respect to intensity-distribution particle size, according to Fig. 5a, suspension CN 3 showed a single peak with values near 700 nm, whereas for suspension CN 4, a distribution in three different ranges was observed, with mean values near to 15 nm and intensity below 1%; 150 nm and maximum intensity of about 5%; and a more significant population (~15%) with an average size of 1.700 nm. The CN 9 suspension showed a bimodal distribution with peaks between 10 and 40 nm and between 100 and 1000 nm, approximately. For number-distribution particle size (Fig. 5b), suspension CN 3 had about 21% of the particles within the 100–400 nm range, CN 4 more than 50% of the particles with dimensions between 15 and 20 nm, and CN 9 with approximately 25% of particles between 15 and 35 nm and less than 5% between 100 and 300 nm. These results show that particle size measurement based on number-distribution size and intensity-distribution size are considerably different, especially for suspensions CN 3 and CN 4, indicating that these suspensions have high size dispersion. This high size dispersion was also observed in microscopy images (Fig. 2), where both micro and nanometric fibers can be seen. In addition, this is also in agreement with the high PDI values for these suspensions. Indeed, based on the PDI values linked to the size distribution shown in Table 5 and in Fig. 5, it is possible to observe that the suspensions obtained under the CN 3 and 9 conditions are more homogeneous.

The CN 3 suspension showed a homogenous micrometric particle-size distribution, with dimensions above 100 nm. Again, this indicates that the low acid concentration (50% w/w) used in CN 3 condition was not enough to release more nanoparticles than micrometric particles, even when the other variables (pulp-to-solution ratio, reaction time and temperature) were set at their highest level. On the other hand, for CN 4 suspension with hydrolysis carried out at a higher acid concentration (60% w/w), a large number of particles smaller than 100 nm in size were obtained. However, the distribution was not homogeneous. For CN 9 suspension obtained when the acid hydrolysis variables were set at their highest level, except for reaction temperature, (64% w/w), high homogeneity was observed as indicated by the lowest PDI determined, and the considerable amount of particles below 100 nm.

3.7. Zeta potential analyses

During the isolation of cellulose nanoparticles by acid hydrolysis using sulfuric acid, the amorphous regions of the cellulose is preferentially hydrolyzed and part of the surface hydroxyl groups are substituted by sulfate groups, conferring a negatively charged group to the particles (Teodoro et al., 2011). This charge on the nanocellulose surface is directly related to the Zeta potential value, which has been reported as a good indicator of the acid hydrolysis effectiveness (Corrêa, Teixeira, Pessan, & Mattoso, 2010; Teodoro et al., 2011) and consequently provides information about the formation of a stable and colloidal suspension. In general, values lower than −15 mV represent the start of particle agglomeration and values higher than −30 mV (absolute value) mean that there is sufficient mutual repulsion, resulting in a colloidal stability (Zhou et al., 2012).

The Zeta potential for CNs from IB fibers (Table 5) was approximately in the range of −22 to −31 mV, which is similar to values obtained for cellulose nanoparticles obtained from cotton (Teixeira et al., 2010) and curaua (Corrêa et al., 2010). Among the three selected suspensions, the Zeta potential was higher in accordance with the concentration of sulfuric acid used (CN 9 > CN 4 > CN 3), indicating the higher effect of the acid concentration on the stability of suspensions. The higher zeta potential of the cellulose nanoparticles in suspension CN 9, indicates the higher stability of the suspension and consequent formation of a colloidal suspension.

4. Conclusions

In this study, cellulose nanoparticles were produced from *Imperata brasiliensis* fibers under different acid hydrolysis conditions according to a Taguchi orthogonal array design. Based on the results of color, stability, crystallinity index, thermal properties, particle size and Zeta potential, cellulose nanoparticles with good physical-chemical

Table 5
Size distribution and Zeta Potential of the CNs 3, 4 and 9.

Samples	CN 3 (nm)			CN 4 (nm)			CN 9 (nm)		
Groups	1°	2°	3°	1°	2°	3°	1°	2°	3°
Intensity	–	120–4000	–	10–20	115–215	1100–2600	15–40	125–1290	–
Number	–	100–400	–	13–20	–	–	15–35	125–300	–
PDI	0.361			0.494			0.305		
Zeta Potential (mV)	−21.86 ± 0.33			−26.90 ± 0.37			−30.83 ± 1.36		

properties were obtained under the following acid hydrolysis conditions: H_2SO_4 64% (w/w) at 35 °C for 75 min with a pulp-to-solution ratio of 1:20 (g/mL). In addition, the nanocellulose obtained from *Imperata brasiliensis* has properties similar to nanocelluloses obtained from other natural resources. Therefore, it could also be applied in areas such as in pharmaceutical industries, electronics components, biomedicine, and as reinforcement for nanocomposites.

Acknowledgments

The authors acknowledge FAPESP (2011/14153-8), CNPq (Proc. 303287/2013-6), CAPES/PVNS CAPES/PNPD for fellowships and financial support. Valdeir Arantes also thanks CNPq and FAPESP (2015/02862-5) for financial support.

References

Adsul, M., Soni, S. K., Bhargava, S. K., & Bansal, V. (2012). Facile approach for the dispersion of regenerated cellulose in aqueous system in the form of nanoparticles. *Biomacromolecules, 13*(9), 2890–2895.

Arrieta, M. P., Fortunati, E., Dominici, F., Rayón, E., López, J., & Kenny, J. M. (2014). Multifunctional PLA −PHB/cellulose nanocrystal films: Processing, structural and thermal properties. *Carbohydrate Polymers, 107*, 16–24.

Barud, H. S., Souza, J. L., Santos, D. B., Crespi, M. S., Ribeiro, C. A., Messaddeq, Y., et al. (2011). Bacterial cellulose/poly (3-hydroxybutyrate) composite membranes. *Carbohydrate Polymers, 83*(3), 1279–1284.

Benini, K. C. C. C., Voorwald, H. J. C., Cioffi, M. O. H., Milanese, A. C., & Ornaghi, H. L., Jr. (2016). Characterization of a new lignocellulosic fiber from Brazil: Imperata brasiliensis (Brazilian satintail) as an alternative source for nanocellulose extraction. *Journal of Natural Fibers, 478*(October), 1–14. http://dx.doi.org/10.1080/15440478.2016.1167647.

Boujemaoui, A., Mongkhontreerat, S., Malmström, E., & Carlmark, A. (2015). Preparation and characterization of functionalized cellulose nanocrystals. *Carbohydrate Polymers, 115*, 457–464. http://dx.doi.org/10.1016/j.carbpol.2014.08.110.

Cao, Y., Jiang, Y., Song, Y., Cao, S., Miao, M., Feng, X., et al. (2015). Combined bleaching and hydrolysis for isolation of cellulose nanofibrils from waste sackcloth. *Carbohydrate Polymers, 131*, 152–158.

Carvalho, M. M., Xavier, D. F., Freitas, V. D. P., & Silva, R. (2000). Correção da Acidez do Solo e Controle do Capim-Sapé Soil Acidity Correction and Control of Sapé-Grass. *Revista Brasileira de Zootecnia, 29*(1), 33–39.

Chen, W., Yu, H., Liu, Y., Chen, P., Zhang, M., & Hai, Y. (2011). Individualization of cellulose nanofibers from wood using high-intensity ultrasonication combined with chemical pretreatments. *Carbohydrate Polymers, 83*(4), 1804–1811.

Corrêa, A. C., de Teixeira, E. M., Pessan, L. A., & Mattoso, L. H. C. (2010). Cellulose nanofibers from curaua fibers. *Cellulose, 17*(6), 1183–1192.

Dai, D., & Fan, M. (2011). Investigation of the dislocation of natural fibres by fourier-transform infrared spectroscopy. *Vibrational Spectroscopy, 55*(2), 300–306. http://dx.doi.org/10.1016/j.vibspec.2010.12.009.

Elazzouzi-Hafraoui, S., Nishiyama, Y., Heux, L., Dubreuil, F., Rochas, C., & Putaux, J. (2008). The shape and size distribution of crystalline nanoparticles prepared by acid hydrolysis of native cellulose. *Biomacromolecules,* 57–65.

French, A. D. (2013). Idealized powder diffraction patterns for cellulose polymorphs. *Cellulose, 21*(2), 885–896.

Frone, A. N., Panaitescu, D. N., Donescu, D., Spataru, C. I., Radovici, C., Trusca, R., et al. (2011). Preparation and characterization of PVA composites with cellulose nanofibrils obtained by ultrasonication. *Bioresources, 6*, 487–512.

Goh, K. Y., Ching, Y. C., Chuah, C. H., Abdullah, L. C., & Liou, N. S. (2015). Individualization of microfibrillated celluloses from oil palm empty fruit bunch: Comparative studies between acid hydrolysis and ammonium persulfate oxidation. *Cellulose, 23*(1), 379–390. http://dx.doi.org/10.1007/s10570-015-0812-y.

Habibi, Y., Lucia, L. A., & Rojas, O. J. (2010). Cellulose nanocrystals: Chemistry, self-assembly, and applications. *Chemical Reviews, 110*(6), 3479–3500.

Jonoobi, M., Harun, J., Shakeri, A., & Misra, M. (2009). Chemical composition, crystallinity, and thermal degradation of bleached and unbleached kenaf bast (Hibiscus cannabinus) pulp and nanofibers. *BioResources, 4*(2), 626–639.

Kargarzadeh, H., Ahmad, I., Abdullah, I., Dufresne, A., Zainudin, S. Y., & Sheltami, R. M. (2012). Effects of hydrolysis conditions on the morphology, crystallinity, and thermal stability of cellulose nanocrystals extracted from kenaf bast fibers. *Cellulose, 19*(3), 855–866.

Kargarzadeh, H., Sheltami, R. M., Ahmad, I., Abdullah, I., & Dufresne, A. (2015). Cellulose nanocrystal: A promising toughening agent for unsaturated polyester nanocomposite. *Polymer (United Kingdom), 56*, 346–357. http://dx.doi.org/10.1016/j.polymer.2014.11.054.

Kaushik, A., Singh, M., & Verma, G. (2010). Green nanocomposites based on thermoplastic starch and steam exploded cellulose nanofibrils from wheat straw. *Carbohydrate Polymers, 82*(2), 337–345.

Lamaming, J., Hashim, R., Leh, C. P., & Sulaiman, O. (2017). Properties of cellulose nanocrystals from oil palm trunk isolated by total chlorine free method. *Carbohydrate Polymers, 156*, 409–416. http://dx.doi.org/10.1016/j.carbpol.2016.09.053.

Lee, H. V., Hamid, S. B. A., & Zain, S. K. (2014). Conversion of lignocellulosic biomass to nanocellulose: Structure and chemical process. *The Scientific World Journal, 2014*, 1–22. http://dx.doi.org/10.1155/2014/631013.

Machado, M. S., Sato, C. E., Mulinari, D. R., Cioffi, M. O. H., & Voorwald, H. J. C. (2009). Avaliação térmica do tratamento alcalino em fibras de sapé utilizadas em compósitos naturais. *Anais do 10 (Congresso brasileiro de polímeros – CBPol*.

Mandal, A., & Chakrabarty, D. (2011). Isolation of nanocellulose from waste sugarcane bagasse (SCB) and its characterization. *Carbohydrate Polymers, 86*(3), 1291–1299.

Mariño, M., Lopes da Silva, L., Durán, N., & Tasic, L. (2015). Enhanced materials from nature: nanocellulose from citrus waste. *Molecules (Basel, Switzerland), 20*(4), 5908–5923. http://dx.doi.org/10.3390/molecules20045908.

Mariano, M., Cercená, R., & Soldi, V. (2016). Thermal characterization of cellulose nanocrystals isolated from sisal fibers using acid hydrolysis. *Industrial Crops and Products, 94*, 454–462. http://dx.doi.org/10.1016/j.indcrop.2016.09.011.

Martins, M. A., Teixeira, E. M., Corrêa, A. C., Ferreira, M., & Mattoso, L. H. C. (2011). Extraction and characterization of cellulose whiskers from commercial cotton fibers. *Journal of Materials Science, 46*(24), 7858–7864.

Mtibe, A., Linganiso, L. Z., Mathew, A. P., Oksman, K., John, M. J., & Anandjiwala, R. D. (2015). A comparative study on properties of micro and nanopapers produced from cellulose and cellulose nanofibres. *Carbohydrate Polymers, 118*, 1–8. http://dx.doi.org/10.1016/j.carbpol.2014.10.007.

Mulinari, D. R., Cioffi, M. O. H., & Voorwald, H. J. C. (2009). Review on natural fibers/HDPE composites: Effect of chemical modification on the mechanical and thermal properties. In F. Willems, & P. Moens (Eds.). *Green composites: Properties, design and lifecycle assessment* (pp. 53–78). New York, USA: Nova Science Publishers Inc.

Ng, H.-M., Sin, L. T., Tee, T.-T., Bee, S.-T., Hui, D., Low, C.-Y., et al. (2015). Extraction of cellulose nanocrystals from plant sources for application as reinforcing agent in polymers. *Composites Part B: Engineering, 75*, 176–200. http://dx.doi.org/10.1016/j.compositesb.2015.01.008.

Niu, F., Li, M., Huang, Q., Zhang, X., Pan, W., Yang, J., et al. (2017). The characteristic and dispersion stability of nanocellulose produced by mixed acid hydrolysis and ultrasonic assistance. *Carbohydrate Polymers, 165*, 197–204. http://dx.doi.org/10.1016/j.carbpol.2017.02.048.

Olaru, A., Malutan, T., Ursesco, C. M., Geba, M., & Stratulat, L. (2016). Structural changes in hemp fibers following temperature, humidity and UV or Gamma-ray radiation exposure. *Cellulose Chemistry and Technology, 50*, 31–39.

Ornaghi, H. L., Jr., Poletto, M., Zattera, A. J., & Amico, S. C. (2014). Correlation of the thermal stability and the decomposition kinetics of six different vegetal fibers. *Cellulose, 21*(1), 177–188.

Oun, A. A., & Rhim, J. W. (2016). Characterization of nanocelluloses isolated from Ushar (Calotropis procera) seed fiber: Effect of isolation method. *Materials Letters, 168*, 146–150. http://dx.doi.org/10.1016/j.matlet.2016.01.052.

Poletto, M., Ornaghi, H. L., Júnior, & Zattera, A. J. (2014). Native cellulose: Structure, characterization and thermal properties. *Materials, 7*(9), 6105–6119. http://dx.doi.org/10.3390/ma7096105.

Qua, E. H., Hornsby, P. R., Sharma, H. S. S., & Lyons, G. (2011). Preparation and characterisation of cellulose nanofibres. *Journal of Materials Science, 46*(18), 6029–6045.

Rosa, M. F., Medeiros, E. S., Malmonge, J. A., Gregorski, K. S., Wood, D. F., Mattoso, L. H. C., et al. (2010). Cellulose nanowhiskers from coconut husk fibers: Effect of preparation conditions on their thermal and morphological behavior. *Carbohydrate Polymers, 81*(1), 83–92.

Rosa, S. M. L., Rehman, N., De Miranda, M. I. G., Nachtigall, S. M. B., & Bica, C. I. D. (2012). Chlorine-free extraction of cellulose from rice husk and whisker isolation. *Carbohydrate Polymers, 87*(2), 1131–1138. http://dx.doi.org/10.1016/j.carbpol.2011.08.084.

Saelee, K., Yingkamhaeng, N., Nimchua, T., & Sukyai, P. (2016). An environmentally friendly xylanase-assisted pretreatment for cellulose nanofibrils isolation from sugarcane bagasse by high-pressure homogenization. *Industrial Crops & Products, 82*, 149–160. http://dx.doi.org/10.1016/j.indcrop.2015.11.064.

Santos, R. M. D., Flauzino Neto, W. P., Silvério, H. A., Martins, D. F., Dantas, N. O., & Pasquini, D. (2013). Cellulose nanocrystals from pineapple leaf: A new approach for the reuse of this agro-waste. *Industrial Crops and Products, 50*, 707–714.

Segal, L., Creely, J. J., Martin, A. E., Jr., & Conrad, C. M. (1959). An empirical method for estimating the degree of crystallinity of native cellulose using the X-ray diffractometer. *Textile Research Journal, 29*, 786–794.

Seo, J.-H., & Kim, H.-J. (2015). Effect of H2O2 bleaching with ultrasonication on the properties of thermomechanical pul and unbleached kraft pulp. *Ultrasonics Sonochemistry, 23*, 347–353.

Shankar, S., & Rhim, J. (2016). Preparation of nanocellulose from micro-crystalline cellulose: The effect on the performance and properties of agar-based composite films. *Carbohydrate Polymers, 135*, 18–26. http://dx.doi.org/10.1016/j.carbpol.2015.08.082.

Sheltami, R. M., Abdullah, I., Ahmad, I., Dufresne, A., & Kargarzadeh, H. (2012). Extraction of cellulose nanocrystals from mengkuang leaves (Pandanus tectorius). *Carbohydrate Polymers, 88*(2), 18–26. http://dx.doi.org/10.1016/j.carbpol.2015.08.082.

Siró, I., & Plackett, D. (2010). Microfibrillated cellulose and new nanocomposite materials: A review. *Cellulose, 17*(3), 459–494.

Souza, R. M., Teixeira, N. M., & Torres, R. A. (1985). Métodos de controle do sapê em pastagem do capim-gordura. *Pesquisa Agropecuária Brasileira, 20*, 963–967.

Spinacé, M. A. S., Lambert, C. S., Fermoselli, K. K. G., & De Paoli, M.-A. (2009). Characterization of lignocellulosic curaua fibres. *Carbohydrate Polymers, 77*(1), 47–53. http://dx.doi.org/10.1016/j.carbpol.2008.12.005.

Tehrani, Z., Nordli, H. R., Pukstad, B., Gethin, D. T., & Chinga-Carrasco, G. (2016). Translucent and ductile nanocellulose-PEG bionanocomposites–A novel substrate with potential to be functionalized by printing for wound dressing applications. *Industrial Crops and Products, 93*, 193–202. http://dx.doi.org/10.1016/j.indcrop.

2016.02.024.
Teodoro, K. B. R., Teixeira, E. D. M., Corrêa, A. C., Campos, A., De Marconcini, J. M., & Mattoso, L. H. C. (2011). Whiskers de fibra de sisal obtidos sob diferentes condições de hidrólise ácida: Efeito do tempo e da temperatura de extração. *Polímeros, 21*(4), 280–285.
Tian, C., Yi, J., Wu, Y., Wu, Q., Qing, Y., & Wang, L. (2016). Preparation of highly charged cellulose nanofibrils using high-pressure homogenization coupled with strong acid hydrolysis pretreatments. *Carbohydrate Polymers, 136*, 485–492.
United States Departament of Agriculture (2017). *ARS-Agricultural research Service, National Genetic Resources Program.* [http://www.ars-grin.gov/cgi-bin/npgs/html/family.pl?2479 (Accessed November 9, 2017)].
Wada, M., & Okano, T. (2001). *Localization of I (and I (phases in algal cellulose revealed by acid treatments.* 183–188.
Wang, L. F., Shankar, S., & Rhim, J.-W. (2017). Properties of alginate-based films reinforced with cellulose fibers and cellulose nanowhiskers isolated from mulberry pulp. *Food Hydrocolloids, 63*, 201–208. http://dx.doi.org/10.1016/j.foodhyd.2016.08.041.
Xiang, Z., Gao, W., Chen, L., Lan, W., & Troy, J. Y. Z. (2016). A comparison of cellulose nanofibrils produced from Cladophora glomerata algae and bleached eucalyptus pulp. *Cellulose, 23*(1), 493–503.
Xiong, R., Han, Y., Wang, Y., Zhang, W., Zhang, X., & Lu, C. (2014). Flexible, highly transparent and iridescent all-cellulose hybrid nanopaper with enhanced mechanical strength and writable surface. *Carbohydrate Polymers, 113*, 264–271. http://dx.doi.org/10.1016/j.carbpol.2014.06.069.
Yu, H., Qin, Z., Liu, Y., Chen, L., Liu, N., & Zhou, Z. (2012). Simultaneous improvement of mechanical properties and thermal stability of bacterial polyester by cellulose nanocrystals. *Carbohydrate Polymers, 89*(3), 971–978.
Zhou, Y. M., Fu, S. Y., Zheng, L. M., & Zhan, H. Y. (2012). Effect of nanocellulose isolation techniques on the formation of reinforced poly (vinyl alcohol) nanocomposite films. *eXPRESS Polymer Letters, 6*(10), 794–804.